Journal of Molecular Spectroscopy 266 (2011) 57–62

Contents lists available at ScienceDirect

Journal of Molecular Spectroscopy

journal homepage: www.elsevier.com/locate/jms

High-resolution spectroscopy of the v_8 band of methylene bromide using a quantum cascade laser

Brian E. Brumfield [a], Jacob T. Stewart [a], Benjamin J. McCall [b,*]

[a] Department of Chemistry, University of Illinois, 600 South Mathews Avenue, Urbana, IL 61801, USA
[b] Departments of Chemistry and Astronomy, University of Illinois, Urbana, IL 61801, USA

ARTICLE INFO

Article history:
Received 28 December 2010
In revised form 12 February 2011

Keywords:
Methylene bromide
Quantum cascade laser
Fresnel rhomb

ABSTRACT

A continuous wave cavity ringdown spectrometer with a Fabry-Perot quantum cascade laser has been used to collect a rotationally-resolved infrared spectrum of the v_8 vibrational band of methylene bromide in a slit nozzle expansion. In our laboratory, previous observations of the vibrational band were limited by spectral coverage to only the P and Q-branches and by the 24 MHz step-size of the laser [1]. The issue of limited spectral coverage has been resolved using a Fresnel rhomb and a wire grid polarizer to protect the laser from the destabilizing effects of back-reflection from the ringdown cavity. The frequency step-size of the spectrometer has been reduced from 24 MHz to 2 MHz. With both of these instrument enhancements, we have been able to record the R-branch of the vibrational band, and can resolve many lines that were previously blended in spectra acquired using a pinhole expansion nozzle. Significant hyperfine splitting was observed for the low-J transitions in the P and R-branches. It was possible to neglect the effects of hyperfine splitting for transitions involving $J'' > 2$ in the spectral assignment, and simulations using the constants obtained by fitting to Watson's S-reduced Hamiltonian for $CH_2{}^{79}Br^{81}Br$, and the A-reduced form for $CH_2{}^{79}Br_2$ and $CH_2{}^{81}Br_2$, provide a good match to experimental spectra. A total of 297 transitions have been assigned for all three isotopologues, with a standard deviation of 0.00024 cm^{-1}($\sim$7 MHz).

1. Introduction

High-resolution gas-phase spectroscopy in the mid-infrared (mid-IR) is useful for studying the fundamental vibrational modes of molecules and molecular clusters. Lead salt diode lasers have been used to collect high-resolution gas-phase spectra of large molecules [2–6] and clusters [7–9] in supersonic expansions. Further development of lead salt diode laser spectrometers is stymied by their limited frequency coverage, low output powers, poor beam quality, and cryogenic operation.

By comparison, quantum cascade lasers (QCLs) offer several significant advantages over lead salt diode lasers. The narrow laser linewidths (<30 MHz), good beam quality, and high cw output powers ($\sim$1–100 mW) make quantum cascade lasers desirable for sensitive, high-resolution spectroscopy applications. The issue of narrow frequency coverage ($\sim$20 cm^{-1}) can be overcome by using an external cavity system [10–12]. Though there is a wealth of literature leveraging the development of QCL spectrometers towards trace gas sensing applications [13], there have been far fewer studies incorporating QCL spectrometers with supersonic expansions [1,14–16].

We are developing a continuous wave cavity ringdown (cw-CRD) spectrometer to acquire a rotationally-resolved, cold, gas-phase spectrum of a vibrational band of buckminsterfullerene (C_{60}) around 8.5 μm. In previously published work we used a supersonic expansion of methylene bromide (CH_2Br_2) seeded in argon to test the sensitivity and resolution of our QCL-based cw-CRD spectrometer [1]. During this testing several problems negatively influenced the sensitivity and resolution of the instrument. The photoconductive mercury–cadmium–telluride (PC-MCT) detector was found to have a slower response time than quoted by the manufacturer. This impaired the fitting of the ringdown decays, leading to a higher than expected noise level. Optical feedback from light rejected by the cavity induced mode-hops during scanning, and may have played a role in reducing the sensitivity of the instrument [17]. A limitation on the current step-size output by the laser power supply led to an undersampling of the methylene bromide lines.

Recently we have been able to modify the instrument to address the concerns mentioned above. To resolve the detector response time issues experienced in the previous study, we have replaced the PC-MCT detector with a photovoltaic mercury–cadmium–telluride (PV-MCT) detector. The influence of optical back-reflection has been mitigated with the addition of a Fresnel rhomb-based optical isolator. We have also decreased the current step-size of

* Corresponding author.
E-mail address: bjmccall@illinois.edu (B.J. McCall).

0022-2852/$ - see front matter © 2011 Elsevier Inc. All rights reserved.
doi:10.1016/j.jms.2011.02.013

our laser power supply, allowing us to sample methylene bromide transitions with several points per line. With our improved spectrometer, we have re-visited our earlier work on the ν_8 vibrational band of methylene bromide with better sensitivity and resolution. The following work highlights the improved instrument performance, and presents a more detailed analysis of the ν_8 vibrational band of methylene bromide for all three isotopologues.

2. Experimental

The experimental layout in this paper is similar to that presented in Brumfield et al. [1] with some modifications detailed below. We use a Fabry-Perot QCL provided by our collaborators at Princeton University.

An ILX Lightwave (LDX-3232) power supply is used to source current to the QCL. Previously, the laser current was controlled through a custom LabWindows program that communicated with the power supply over a GPIB interface. Communication over the GPIB limited the current step-size to 0.1 mA, corresponding to a frequency step-size of ~24 MHz. This limitation was overcome by using the external modulation input of the power supply. At the start of a scan the laser is brought to an initial current using the GPIB interface. A voltage output from a data acquisition (DAQ) board, which can be scanned from 0 to a maximum of 10 V, is fed into a homemade 30:1 voltage divider before entering the external modulation input. The voltage divider is used to reduce the electrical noise coupled into the cable between the DAQ board output and the power supply modulation input. During spectral acquisition the current is stepped by increasing the applied voltage to the modulation input. Using this method methylene bromide spectra were acquired with ~2 MHz frequency steps.

Infrared light exiting the QCL is collimated by a series of lenses and then passed through a Ge acousto-optic modulator (AOM). The zero order beam is sent to the reference arm of the experiment, which is comprised of a wavemeter and a 40 cm absorption cell filled with ~4 Torr of SO_2. The zero order beam is passed through the absorption cell in a triple-pass configuration to achieve a higher S/N on the SO_2 absorption features.

After sample ringdown collection, the computer sends a signal to turn off the AOM. The duration of this delay depends on whether or not a wavemeter reading will be acquired with the direct absorption cell data. For recording a frequency reading with the wavemeter, it was found that delaying 7 s after turning off the AOM provided a stable reading. This long delay is due to the limited time response of an auto-gain circuit in the wavemeter. To save time during data acquisition the wavemeter is only used every 10–50 data points. After reference data is collected the applied modulation input voltage is stepped and the process is repeated.

The first order beam passes through a wire grid polarizer (ThorLabs WP25H-B) and a ZnSe quarter wave rhomb (II-VI Infrared FRZ-8.4-.55-90-90RM). The polarizer is set to pass the horizontal polarization of the laser light. Light exiting the polarizer then passes through the quarter wave rhomb and exits as circularly polarized light. Any light that is reflected by the input ringdown mirror has the handedness of its circular polarization reversed, and upon transmission back through the rhomb is converted into vertically polarized light. The vertically polarized light is then attenuated by the ~400:1 extinction coefficient of the wire grid polarizer. This provides a potential maximum optical isolation of ~25 dB against optical back-reflection, but the achieved experimental isolation was likely less than this due to alignment errors and the actual retardation provided by the rhomb. Experimentally, the rhomb has provided sufficient protection against optical back-reflection to reduce the number of mode-hops experienced during scanning. A similar optical isolation scheme has been used with a lead salt diode laser heterodyne spectrometer [18].

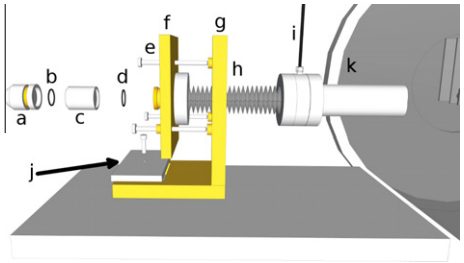

Fig. 1. Diagram showing a close-up of one of the new ringdown mounts used to form our cavity: (a) ringdown mirror in two piece aluminum holder, o-ring seal made between mirror HR surface and rightmost piece of the mirror holder, (b) o-ring for making a vacuum seal between ringdown mirror holder and piezoelectric transducer, (c) piezoelectric transducer, (d) o-ring for making a seal between the piezoelectric transducer and kinematic portion of brass mount, (e) knob adjustment screws, (f) brass kinematic plate, (g) stationary portion of brass mount, (h) metal bellows with 2 $\frac{3}{4}''$ conflat connections to the kinematic brass plate and the CF assembly connected to the half-nipple welded directly to the vacuum chamber, (i) purge gas line, (j) aluminum compression plate to secure stationary part of brass mount, (k) welded CF half-nipple extending from vacuum chamber.

After passing through the Fresnel rhomb the laser light is coupled into the ~85 cm long ringdown cavity (FSR ~ 176 MHz) using a three lens telescope. We recently acquired two new high reflectivity mirrors (Los Gatos 901-0010-8300) with 1 m radii of curvature to form our high finesse cavity. The planar side of the mirrors have an 8–12 μm broadband AR coating. New mirror mounts (shown in Fig. 1) were designed to minimize the impact of anisotropic thermal expansion of the vacuum chamber when it is under a heat load from our high-temperature oven expansion source. Each ringdown mirror is held in a two piece holder machined from aluminum. Direct contact between the piece of the aluminum holder pressed against the AR side of the mirror is cushioned by a teflon gasket. A vacuum seal is maintained on the HR side of the mirror by an o-ring seated in a groove on the second piece of the aluminum holder. This o-ring seal is not shown in Fig. 1. The mirror holder then threads onto the end of a piezoelectric transducer (PZT). A vacuum seal is formed by an o-ring (b) compressed between (a) and (c). The PZT threads onto the end of the brass kinematic plate (f). The brass kinematic plate has an o-ring groove machined onto the end, forming a vacuum seal between (c) and (f). The opposite side of the kinematic plate has a machined knife edge to create a Conflat (CF) seal with the long bellows (h). The mirror is aligned by using knob adjustment screws (e). The springs providing the restoring force holding the kinematic plate to the stationary part of the brass holder are not shown in Fig. 1. The stationary portion of the holder (g) is secured to the optics breadboard platform by compression using an aluminum plate with a through-hole for a $\frac{1}{4}$–20 screw. This made it possible to compress a sorbathane sheet between (g) and the breadboard platform. A 4″ long bellows (h) provides a flexible connection that maintains the vacuum between the ringdown mirror and the chamber by 2 $\frac{3}{4}''$ Conflat connections. The mirrors are protected from chamber dust by using the purge gas lines (i). The other ringdown mirror mount is the same as that shown in Fig. 1, but does not have the PZT (c) or o-ring (b).

We create a supersonic expansion from a 12 mm × 150 μm × 7 mm (length × width × channel depth) slit that has been machined into a 1 $\frac{1}{3}''$ conflat blank. In the previous study we used an 800 μm pinhole nozzle [1]. The backing pressure for the expansion is provided by two flow controllers, one that is fed by argon that has passed through a bubbler with methylene bromide (Aldrich 99% purity), and another drawing straight from an argon cylinder (S.J. Smith 99.95% purity). Gas exiting the flow controllers

is split to a continuous dump provided by a Welch pump and to a solenoid valve. The solenoid valve (Parker Hannifin 9S1-A1-P1-9B07) controls the flow of gas to the supersonic expansion source. When the valve is open data is taken with the jet and sample present. When the valve is closed a background spectrum is taken in the absence of the jet and sample. The delay for data acquisition between open and closed states of the valve was 2 s, and is controlled by the computer. The data was collected this way so fringing that was normally present during data collection could be subtracted. As a result of this collection process, scanning proceeded slowly at a rate of ~0.05 cm^{-1} per hour. The frequency drift of the QCL is <0.006 cm^{-1} after the laser has been on for an hour. This slow temperature drift is likely due to the temperature equilibration of the laser and cryostat mount. An example of the fringe subtraction is shown in Fig. 2.

The period and amplitude of the fringing is sensitive to the optical alignment. The frequency of the fringing falls between 400 and 600 MHz. The amplitude of the fringing varied between ~10^{-5} and 10^{-6} fractional loss per pass. All the lenses and infrared detectors in the experiment have been tilted to try to minimize etalon effects.

We have implemented a new homemade driver for the piezoelectric transducer using an audio amplifier (Samson Servo 300). Our new driver can sweep the cavity over one free spectral range at a repetition frequency greater than 250 Hz, which is a significant improvement over our previous driver's performance (<80 Hz). The ringdown collection rate varied between 50 and 200 ringdowns/s, and was dependent on the quality of the cavity alignment and the comparator trigger level setting.

Light leaking out of the cavity is focused onto a PV-MCT detector (Kolmar Technologies KMPV11-1-J1/AC). The signal from the PV-MCT is post-amplified (Kolmar Technologies KA100-E2/AC) by a factor of 20 V/V, and sent into a homemade comparator triggering circuit and a 14-bit high speed digitizer to be recorded for later processing.

When a cavity build-up event meets the comparator threshold, the comparator sends a signal to trigger the high-speed digitizer to record data. Simultaneously the computer sends out a signal to turn off the AOM so light is not being coupled into the cavity while the ringdown decay is being collected. Two sets of 100 ringdowns per point are collected per modulation voltage step because of the sample and background subtraction from the supersonic jet.

3. Results and discussion

The ν_8 band of methylene bromide was acquired from 1196.14 to 1197.92 cm^{-1}. Fig. 3 shows the experimental data collected over this range plotted with our simulation of the band. The total frequency coverage of the vibrational band was 1.78 cm^{-1}. Previously we covered 1.75 cm^{-1} of the methylene bromide band using a pinhole nozzle [1]. This prior coverage only spanned the Q and P-branches of the vibrational band because it was not possible to get reliable mode-hop free spectral coverage beyond 1197 cm^{-1} due to back-reflection induced instability. By using the Fresnel rhomb optical isolator we were able to center our spectral coverage over the band center and record portions of both the P and R-branches.

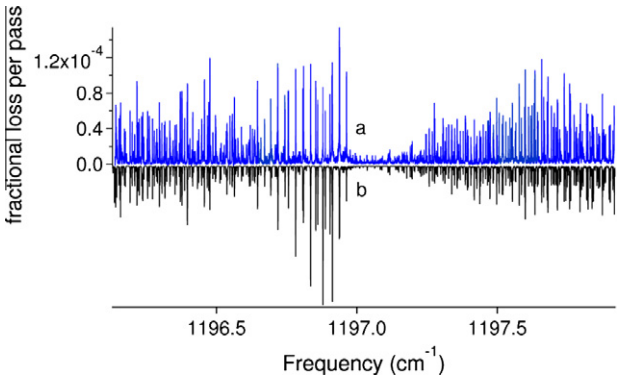

Fig. 3. Trace (a) is the experimental spectrum. Trace (b) is a simulated spectrum resulting from the assignment and fitting of the vibrational band. Trace (b) is composed of two co-added simulations created using PGOPHER [19]. One is a simulation with T_{rot} = 20 K and linewidths of 0.00045 cm^{-1} for jet-cooled methylene bromide. The second simulation is for the residual background sample contribution with T_{rot} = 300 K and linewidths of 0.0011 cm^{-1}. The 300 K simulation is scaled by a factor of 1.5 with respect to the 20 K simulation in the co-addition.

To properly simulate our experimental data, it was necessary to include a room temperature contribution because residual methylene bromide was present in the vacuum chamber. This residual sample is present because the solenoid pulse open duration is on the order of a second. It should be noted that Trace (a) in Fig. 3 is composed of many spectra spanning 0.08–0.34 cm^{-1} that were independently calibrated; Fig. 4 provides an example of one of these spectra.

The distance from the slit nozzle to the cavity axis was ~6 mm for all scans. For all scanning windows a flow rate of 75 sccm of Ar bubbled through methylene bromide and 1500 sccm of pure Ar were used. With these flow rates, when the solenoid valve was open the pressure in our vacuum chamber would rise to 70–90 mTorr.

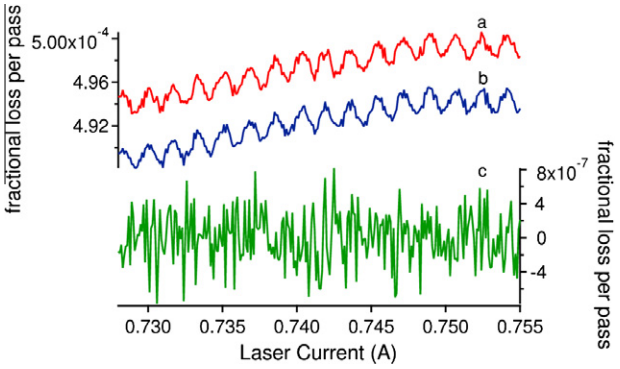

Fig. 2. Ringdown spectra of fractional loss per pass versus laser current illustrating effectiveness of background subtraction to remove fringing. There was no sample present in the expansion during this scan. Traces (a) and (b) are recorded with the jet on and off respectively. Trace (a) is offset to ease comparison with Trace (b). Trace (c) is the subtracted result from Traces (a) and (b).

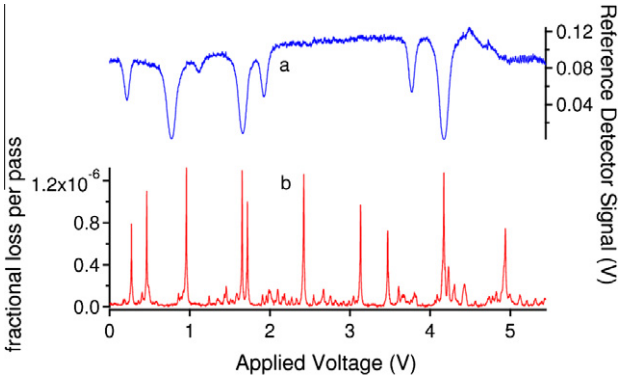

Fig. 4. Trace (a) is the signal from the direct absorption cell filled with SO_2 used for absolute frequency calibration. Trace (b) is the fringe subtracted cavity ringdown spectrum of a portion of the methylene bromide Q-branch. Both traces are plotted against the voltage applied to the modulation input on the laser power supply.

To calibrate our spectra, we utilized the wavemeter for relative frequency calibration, and SO_2 lines for absolute frequency calibration. Wavemeter data were fit to a 4th order polynomial, which was used to convert the voltage applied to the modulation input into a frequency scale. The SO_2 reference scan was then plotted against the wavemeter frequency scale. Each of the reference lines was fit to a Gaussian profile. From the Gaussian fitting a line center position calibrated to the wavemeter frequency is obtained. Because the wavemeter is intentionally misaligned, to reduce back-reflections to the QCL, there exists a frequency offset between the true frequency and that provided by the wavemeter. This offset was generally found to be between 100 and 300 MHz, and was dependent on the wavemeter alignment. To determine this offset, the difference between the wavemeter calibrated frequency and the HITRAN2008 [20] transition frequency is calculated for all the observed reference lines. All these offset values are averaged, and the resulting average is added to the wavemeter calibration, generating an absolute frequency scale for the methylene bromide spectra. The 40 MHz Bragg downshift of the AOM is also accounted for in the calibration procedure.

Overlap between individual spectra after calibration is usually good, with a difference <15 MHz. In the worst cases, the difference can be as large as 30 MHz; this is possibly limited by the uncertainty and systematic errors that exist for the SO_2 reference data in HITRAN2008 [20]. In the HITRAN2008 database, the listed uncertainty in the line positions is in the range of 3–30 MHz. In addition to these issues, some of the residuals resulting from fitting the wavemeter traces provide evidence of periodic drifting in the laser frequency less than or equal to 24 MHz. Such drifts could be explained by gradual changes in the laser temperature <0.01 K. The laser temperature control loop is not capable of correcting for such small temperature changes.

Previous work we carried out on the ν_8 band of methylene bromide was done using a pinhole nozzle expansion source [1]. Using a slit nozzle in this study provided narrower linewidths at the expense of a warmer rotational temperature. In our previous work the linewidth was around 45 MHz (0.0015 cm^{-1}), and many of the closely spaced methylene bromide lines for the three isotopologues were blended and not assignable. The narrowest transitions seen in the current work are 13.5 MHz (0.00045 cm^{-1}), which has allowed us to assign many more transitions. Assignment of the ν_8 band was initially guided by our previous assignment [1], which was refined using the new spectra. The band was then simulated using PGOPHER [19]. Methylene bromide is a near prolate top with a ground state $\kappa \sim -0.996$, and fitting was done to the A-reduced form of the asymmetric top Hamiltonian for $CH_2{}^{79}Br_2$ and $CH_2{}^{81}Br_2$, while the S-reduced form was used for $CH_2{}^{79}Br^{81}Br$. The choice of reduction was based on the availability of the ground state constants provided in microwave spectroscopy studies of methylene bromide [21,22]. The I^r representation was used for all three isotopologues. Nuclear spin statistical weights of 9:7:7:9 (J_{ee}:J_{eo}:J_{oe}:J_{oo}) were included for the $CH_2{}^{79}Br_2$ and $CH_2{}^{81}Br_2$ isotopologues. The $CH_2{}^{79}Br^{81}Br$ isotopologue lacks nuclear spin statistics because of its lower symmetry. Because of the nearly equal abundance of ^{79}Br and ^{81}Br, a 1:2:1 abundance of $CH_2{}^{79}Br_2$:$CH_2{}^{79}Br^{81}Br$:$CH_2{}^{81}Br_2$ exists in the sample. This ratio was accounted for in the simulation. Only the excited vibrational state constants ν_0, A', B', C', and $D'_K(\Delta'_K)$ were allowed to float during the fitting process, while the ground state constants were fixed to their values determined through microwave spectroscopy [21,22]. For $CH_2{}^{79}Br^{81}Br$, the value of D''_K is not known, so instead the value of $\Delta D_K = D'_K - D''_K$ was determined in the fitting process. The results of fitting the excited state spectroscopic constants are shown for $CH_2{}^{79}Br^{81}Br$ in Table 1, and for $CH_2{}^{79}Br_2$ and $CH_2{}^{81}Br_2$ in Table 2. The linelist for the assigned transitions is provided in the Supplementary material for this article.

Table 1
Listing of spectroscopic constants for the ν_8 vibrational band of $CH_2{}^{79}Br^{81}Br$ obtained by fitting to Watson's S-reduced form of the asymmetric top Hamiltonian [23]. Spectroscopic constants determined in this work are presented for each isotopologue under the "Current" column. Results of fitting from Brumfield et al. [1] are listed under the "Previous" column. The rotational constants fixed in the ground state are provided under the "Microwave" column. The units for the spectroscopic constants and the standard deviation are in wavenumbers (cm^{-1}). The 1σ uncertainties resulting from the fit are provided in parentheses at the end of each value.

	$CH_2{}^{79}Br^{81}Br$		
	ν_8=1		ν_8=0
	Previous [1]	Current	Microwave[a][22]
ν_0	1196.95797(12)	1196.957052(37)	
A	0.8626649(28)	0.8626518(25)	0.86751916(86)
B		0.0408228(16)	0.040804716(73)
C		0.0392382(14)	0.039253679(87)
ΔD_K[b]		$-2.17(22) \times 10^{-7}$	
D_J[c]			$7.75(25) \times 10^{-9}$
D_{JK}[c]			$-3.81(16) \times 10^{-7}$
d_1[c]			$-6.44(90) \times 10^{-10}$
d_2[c]			$-1.03(1.03) \times 10^{-9}$
# Assigned transitions	22	123	
Standard deviation	0.00044	0.00023	

[a] Rotational constants provided from microwave spectroscopy are for the ground state.
[b] $\Delta D_K = D'_K - D''_K$
[c] Parameter in upper state fixed to values determined from microwave spectroscopy on ground state.

The standard deviation presented in the table is defined as [19]:

$$\text{standard deviation} = \sqrt{\frac{\sum_i^{n_{obs}} (\text{obs}_i - \text{calc}_i)^2}{n_{obs} - n_{para}}} \quad (1)$$

where the total number of assigned transitions is n_{obs}, obs_i is the observed frequency position for the ith assigned transition, calc_i is the calculated frequency position for the ith transition, and n_{para} is the number of parameters floated in the least squares fitting of the spectroscopic data. The standard deviation values for the pinhole expansion work were also presented in Brumfield et al. [1], but they were mislabeled as the average |obs − calc|.

To evaluate the relative accuracy of the frequency calibration for the infrared spectra, a combination differences analysis was carried out using the infrared spectral assignments for the $CH_2{}^{79}Br^{81}Br$ isotopologue. The residuals between the 27 combination differences from the infrared data and ground state data simulated using the rotational constants from Niide et al. [22] were obtained. The standard deviation for the combination differences residuals is 0.00037 cm^{-1}, with a mean of 3.4×10^{-5} cm^{-1}. The resulting standard deviation is within a factor of 2 of the standard deviation results from the fit, and may be larger because of the smaller sample size of the combination differences in comparison to the number of assigned lines in the fit.

The increase in the number of assignments for P and R-branch transitions compared to the previous work allowed for additional excited state parameters to be fit. The failure of the current values of ν_0 to agree within their listed fit uncertainties between both studies is likely due to the use of HITRAN2004 [24] SO_2 line positions in the previous paper. A majority of the HITRAN2008 SO_2 line positions from 1197.00 to 1196.70 cm^{-1} are red-shifted by 20–30 MHz with respect to the frequency positions listed in HITRAN2004. This also explains the systematic red-shift in ν_0 compared the values from the previous study. The addition of D'_K for $CH_2{}^{79}Br_2$ and $CH_2{}^{81}Br_2$ (ΔD_K for $CH_2{}^{79}Br^{81}Br$) as a floated parameter for fitting the newest data is the reason why the values of A'

Table 2
Listing of spectroscopic constants for the ν_8 vibrational band of $CH_2{}^{79}Br_2$ and $CH_2{}^{81}Br_2$ obtained by fitting to Watson's A-reduced form of the asymmetric top Hamiltonian [23]. Spectroscopic constants determined in this work are presented for each isotopologue under the "Current" column.

	$CH_2{}^{79}Br_2$			$CH_2{}^{81}Br_2$		
	ν_8=1		ν_8=0	ν_8=1		ν_8=0
	Previous [1]	Current	Microwave[a] [21]	Previous [1]	Current	Microwave[a] [21]
ν_0	1196.98363(99)	1196.982565(56)		1196.93206(12)	1196.931350(46)	
A	0.8634519(22)	0.8634374(31)	0.868441(13)	0.8619108(23)	0.8618897(32)	0.86675642(56)
B		0.0413299(24)	0.041313137(47)		0.0403157(14)	0.040297341(27)
C		0.0397103(22)	0.039725549(53)		0.0387663(13)	0.038782329(30)
Δ_K		$1.2676(22)\times10^{-5}$	1.2922×10^{-5}[c]		$1.2667(33)\times10^{-5}$	$1.2879(15)\times10^{-5}$
Δ_J[b]			7.9321×10^{-9}[c]			$7.5662(40)\times10^{-9}$
Δ_{JK}[b]			$-3.8403(70)\times10^{-7}$			$-3.7483(20)\times10^{-7}$
δ_J[b]			$5.2279(63)\times10^{-10}$			$4.8773(70)\times10^{-10}$
δ_K[b]			3.93×10^{-8} [c]			$3.782(50)\times10^{-8}$
# Assigned transitions	20	92		20	82	
Standard deviation	0.00035	0.00027		0.00044	0.00022	

[a] Rotational constants provided from microwave work are for the ground state.
[b] Parameter in upper state fixed to values determined from microwave spectroscopy on the ground state.
[c] This parameter was constrained in the microwave work and has no reported uncertainty.

between the two studies do not agree within their listed uncertainties.

We observed complex hyperfine splitting in the low-J P and R-branch features due to the presence of the two bromine nuclei in the molecule (see Fig. 5). The presence of significant hyperfine splitting in methylene bromide was discussed in previous microwave work [25,26,22], and it was emphasized that the low-J transitions present the most complex splitting [26]. Modeling of the complex hyperfine splitting is beyond the scope of this current work, and we did not assign the $P(1)$, $R(0)$, or $R(1)$ transitions.

However, at higher J the microwave work showed that the hyperfine splitting simplified to a triplet pattern, with the peak close to the center of where a transition would be expected without the influence of hyperfine splitting [25,26]. Fig. 6 shows the occurrence of triplet patterns in a section of the R-branch spectrum for all three isotopologues. Transitions assigned with this triplet pattern are marked in the linelist included as Supplementary material to this article. Here it is assumed that the structure seen in the transition is due to hyperfine splitting, and that the asymmetry splitting of the two overlapped transitions is not resolvable given the instrument resolution. Fewer, but similar patterns are found in spectra acquired in the P-branch. In some situations a P-branch transition is seen that is broader than would be expected given the experimental linewidth, and it is likely that this broadening is the result of unresolved hyperfine splitting.

Fig. 7 shows experimental spectra acquired farther from the band center. The simulation and the experimental spectrum are in good agreement despite neglecting hyperfine interactions.

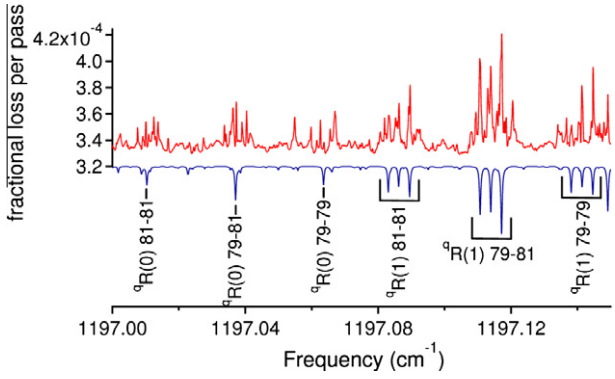

Fig. 5. The top trace is an experimental spectrum of the R-branch. The bottom trace is a section of the simulation shown in Fig. 3. The transitions in the simulation are labeled based on the isotopologue assuming no hyperfine splitting.

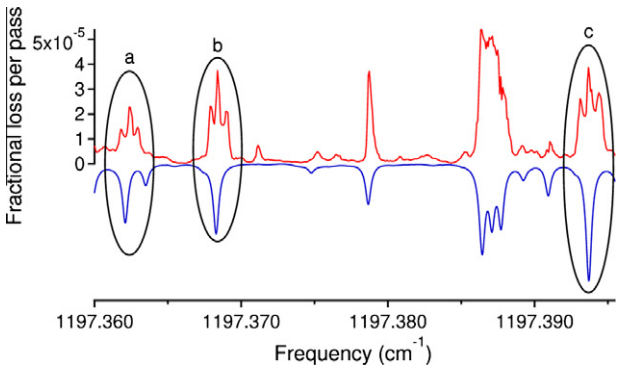

Fig. 6. The top trace is an experimental spectrum of the R-branch spanning 1197.360–1197.395 cm^{-1}. The bottom trace is a section of the simulation shown in Fig. 3. The simulated transitions paired with the triplet patterns observed in the experimental spectrum are circled. The central peak of (a) has been assigned to $^qR_{3,3}(5)$ and $^qR_{3,2}(5)$ of $CH_2{}^{81}Br_2$. The central peak of (b) has been assigned to $^qR_{2,2}(4)$ and $^qR_{2,3}(4)$ of $CH_2{}^{79}Br_2$. The central peak of (c) has been assigned to $^qR_{3,3}(5)$ and $^qR_{3,2}(4)$ of $CH_2{}^{79}Br^{81}Br$.

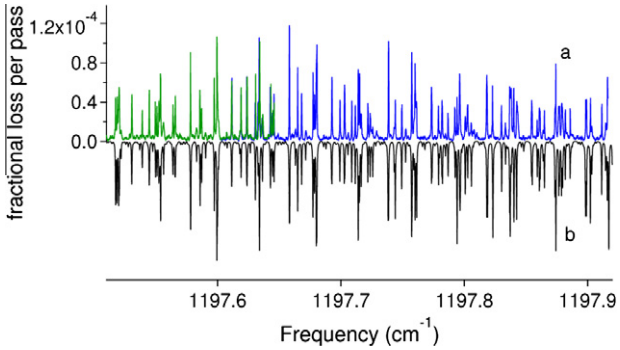

Fig. 7. Trace (a) shows two overlapped cavity ringdown spectra covering 1197.51–1197.92 cm^{-1} in the R-branch. Trace (b) is a section of the simulation shown in Fig. 3.

4. Conclusions

Recent improvements to our QCL cw-CRD spectrometer have led to an increase in the resolution and sensitivity of the instrument. As a result of these improvements, the ν_8 band of methylene

bromide was re-visited and previous spectral assignments were refined, while the total number of assignments was expanded from 62 to 297. The increase in resolution and spectral coverage revealed the presence of complex hyperfine splitting for the $P(1)$, $R(0)$, and $R(1)$ transitions that could not be assigned. Despite the absence of the low-J assignments, fitting of the bulk of the vibrational band was carried out successfully with a standard deviation of 0.00024 cm^{-1}. This study illustrates the suitability of QCL-based spectrometers for high-resolution mid-IR jet spectroscopy.

Acknowledgments

The authors wish to thank Matt Escarra and Professor Claire Gmachl from the Electrical Engineering Department at Princeton University for providing the quantum cascade lasers used in this work. Funding for this research was provided by a Packard Fellowship through the David and Lucile Packard Foundation. Jacob T. Stewart has been supported by a Robert C. and Carolyn J. Springborn Fellowship from the University of Illinois. The authors also wish to thank Professor Kevin Lehmann for suggesting the use of a Fresnel rhomb to build an optical isolator for the QCL spectrometer.

Appendix A. Supplementary data

Supplementary data associated with this article can be found, in the online version, at doi:10.1016/j.jms.2011.02.013.

Supplementary data for this article are available on ScienceDirect (www.sciencedirect.com) and as part of the Ohio State University Molecular Spectroscopy Archives (http://library.osu.edu/sites/msa/jmsa_hp.htm).

References

[1] B.E. Brumfield, J.T. Stewart, S.L.Widicus Weaver, M.D. Escarra, S.S. Howard, C.F. Gmachl, B.J. McCall, Rev. Sci. Instrum. 81 (2010) 063102.
[2] P. Asselin, P. Soulard, L. Manceron, V. Boudon, G. Pierre, J. Mol. Spectrosc. 517–518 (2000) 145–155.
[3] G.M. Hansford, P.B. Davies, J. Gang, D.K. Russell, Spectrochim. Acta Part A 53 (1997) 1755–1759.
[4] P.R. Brown, P.B. Davies, G.M. Hansford, N.A. Martin, J. Mol. Spectrosc. 158 (1993) 468–478.
[5] P.B. Davies, G.M. Hansford, T.C. Killian, J. Mol. Spectrosc. 163 (1994) 138–158.
[6] J. Gang, M. Pennington, D.K. Russell, F.J. Basterrechea, P.B. Davies, G.M. Hansford, J. Opt. Soc. Am. B 11 (1994) 184–190.
[7] H. Qian, W.A. Herrebout, B.J. Howard, Mol. Phys. 91 (1997) 689–696.
[8] M. Wangler, D. Roth, I. Pak, G. Winnewisser, P. Wormer, A. van der Avoird, J. Mol. Spectrosc. 222 (2003) 109–120.
[9] G. Winnewisser, T. Drascher, T. Giesen, I. Pak, F. Schiilling, R. Schieder, Spectrochim. Acta Part A 55 (1999) 2121–2142.
[10] B.G. Lee, M.A. Belkin, R. Audet, J. MacArthur, L. Diehl, C. Pflugl, F. Capasso, D.C. Oakley, D. Chapman, A. Napoleone, D. Bour, S. Corzine, G. Hofler, J. Faist, Appl. Phys. Lett. 91 (2007) 231101–231103.
[11] G. Wysocki, R. Lewicki, R. Curl, F. Tittel, L. Diehl, F. Capasso, M. Troccoli, G. Hofler, D. Bour, S. Corzine, R. Maulini, M. Giovannini, J. Faist, Appl. Phys. B: Lasers Opt. 92 (2008) 305–311.
[12] R. Maulini, I. Dunayevskiy, A. Lyakh, A. Tsekoun, C. Patel, L. Diehl, C. Pflugl, F. Capasso, Electron. Lett. 45 (2009) 107–108.
[13] A. Kosterev, G. Wysocki, Y. Bakhirkin, S. So, R. Lewicki, M. Fraser, F. Tittel, R. Curl, Appl. Phys. B: Lasers Opt. 90 (2008) 165–176.
[14] J.F. Kelly, A. Maki, T.A. Blake, R.L. Sams, J. Mol. Spectrosc. 252 (2008) 81–89.
[15] Y. Xu, X. Liu, Z. Su, R.M. Kulkarni, W.S. Tam, C. Kang, I. Leonov, L. D'Agostino, Proc. SPIE 7222 (2009) 722208–722211.
[16] J. Krieg, V. Lutter, F.X. Hardy, S. Schlemmer, T.F. Giesen, J. Chem. Phys. 132 (2010) 224306.
[17] G.N. Rao, A. Karpf, Appl. Opt. 49 (2010) 4906–4914.
[18] R. Schieder, Infrared Phys. Technol. 35 (1994) 477–486.
[19] C.M. Western, Pgopher, a program for simulating rotational structure, 2010. <http://pgopher.chm.bris.ac.uk>.
[20] L. Rothman, I. Gordon, A. Barbe, D. Benner, P. Bernath, M. Birk, V. Boudon, L. Brown, A. Campargue, J.-P. Champion, K. Chance, L. Coudert, V. Dana, V. Devi, S. Fally, J. Flaud, R. Gamache, A. Goldman, I. Jacquemart, D. Kleiner, N. Lacome, W. Lafferty, J. Mandin, S. Massie, S. Mikhailenko, C. Miller, N. Moazzen-Ahmadi, O. Naumenko, A. Nikitin, J. Orphal, V. Perevalov, A. Perrin, A. Predoi-Cross, C. Rinsland, M. Rotger, M. Šimečková, M. Smith, K. Sung, S. Tashkun, J. Tennyson, R. Toth, A. Vandaele, J. Vander Auwera, J. Quant. Spectrosc. Radiat. Transfer 110 (2009) 533–572.
[21] R.W. Davis, M.C.L. Gerry, J. Mol. Spectrosc. 109 (1985) 269–282.
[22] Y. Niide, H. Tanaka, I. Ohkoshi, J. Mol. Spectrosc. 139 (1990) 11–29.
[23] J. Watson, Vibrational Spectra and Structure, vol. 6, Elsevier, 1977, pp. 2–89.
[24] L. Rothman, D. Jacquemart, A. Barbe, D. Chris Benner, M. Birk, L. Brown, M. Carleer, C. Chackerian Jr., K. Chance, L. Coudert, V. Dana, V. Devi, J.-M. Flaud, R. Gamache, A. Goldman, J.-M. Hartmann, K. Jucks, A. Maki, J.-Y. Mandin, S. Massie, J. Orphal, A. Perrin, C. Rinsland, M. Smith, J. Tennyson, R. Tolchenov, R. Toth, J. Vander Auwera, P. Varanasi, G. Wagner, J. Quant. Spectrosc. Radiat. Transfer 96 (2005) 139–204.
[25] D. Chadwick, D.J. Millen, Trans. Faraday Soc. 67 (1971) 1539–1550.
[26] D. Chadwick, D.J. Millen, Trans. Faraday Soc. 67 (1971) 1551–1568.